Journal of Catalysis **208,** 124–138 (2002)
doi:10.1006/jcat.2002.3548, available online at http://www.idealibrary.com on IDEAL®

Mo Loading Effects over Mo/Si : Ti Catalysts in the Oxidative Dehydrogenation of Ethane

Rick B. Watson and Umit S. Ozkan[1]

Department of Chemical Engineering, The Ohio State University, Columbus, Ohio 43210

Received September 19, 2001; revised January 30, 2002; accepted January 30, 2002

A series of molybdena catalysts (0–20 wt% loadings) were studied with regard to their activity for the oxidative dehydrogenation (ODH) of ethane. Catalysts with single oxide supports of silica and titania were also examined. X-ray diffraction, Raman spectroscopy (ambient and dehydrated conditions), and X-ray photoelectron spectroscopy were used to determine the nature of the molybdena phases supported over the mixed oxide support. Initially, MoO_x preferentially supports on titania. However, interaction with silica is present even at the lowest wt% loading. With increased wt% loading, MoO_x increasingly interacts with the silica phase of the support as titania increasingly segregates into larger anatase domains. Since MoO_x species may share several types of support ligands with differing electronegativity, one cannot adequately describe MoO_x species as being supported exclusively on SiO_2 or TiO_2 domains but rather, as indicated by the Raman results, as being supported on a mix of both species. The structural differences are reflected in ODH reaction performance. The ethylene yield increases with Mo loading over Si : Ti 1 : 1 to a maximum at 10% Mo/Si : Ti 1 : 1, where there may exist an optimum coverage of MoO_x that shares several types of support ligands from both silica and titania domains of the support. The desorption behavior of products formed following ethane adsorption was studied with Mo wt% loading using temperature-programmed desorption.

Key Words: **ethane oxidative dehydrogenation; silica–titania mixed oxides; molybdenum; XPS; Raman spectroscopy.**

1. INTRODUCTION

Because alkanes are relatively inexpensive and are abundant side products of refineries and natural resources such as natural gas, one of their potential uses is in conversion to alkenes (1). Alkenes are heavily used as feedstock in industry, but are more expensive and less available than alkanes. A method that has been widely used to achieve this conversion is steam cracking of alkanes at high temperatures. This method is constrained in many ways, namely, by thermodynamic limitations, by endothermic reactions that require a large input of heat, and by formation of coke on the catalyst (2). Because of these limitations, many research studies have focused on the oxidative dehydrogenation (ODH) of alkanes. ODH is a desirable alternative because, when a proper catalyst is selected, the reaction occurs at lower temperatures and is exothermic, preventing heat input requirements.

Research on ethane ODH catalysts usually falls into two operating temperature categories, above or below the temperature at which significant gas-phase reaction mechanisms participate. Lower temperature catalysts usually consist of reducible transition metal oxides, such as vanadium or molybdenum, and are considered to proceed via a surface mechanism. The higher temperature catalysts do not contain easily reducible ions and consist of Mg, Li, or other group IA or IIA ions or oxides. Several researchers proposed a high-temperature surface/gas-phase mechanism that involves ethyl radical formation by surface oxygen and the subsequent transformation to ethylene through a surface ethoxide intermediate. Whether this oxygen species is adsorbed from the gas phase or from part of the lattice is a current matter of investigation on different types of catalysts that operate by a nonredox mechanism (3).

A redox mechanism exists over reducible metal oxides at lower temperatures of operation (<600°C). The redox mechanism of ethane ODH is generally accepted to occur by a Mars and van Krevelen mechanism (4). The rate-determining step is the abstraction of one H from a C–H bond by lattice oxygen. It is important to note that, in this scheme, often no differentiation is made as to which types of lattice oxygen species at the surface are involved in C–H bond activation. Over supported transition metal oxides, several species may exist in the form of M=O, M–O–M, or M–O-support bonds, where M is the transition metal of interest. The chemical nature of the active oxygen species and the redox properties will play a critical role in catalyst performance and will certainly depend on transition metal loading, dispersion, and support effects. For an optimum combination of activity and selectivity, there should exist a balance between the activation of the hydrocarbon and the ease of removal of oxygen from the catalyst surface. Oxygen that is too tightly bound will result in low activity, while a catalyst with oxygen that is too labile will be

[1] To whom correspondence should be addressed. Fax: (614) 292-3769. E-mail: ozkan.1@osu.edu.

0021-9517/02 $35.00

very active but not selective. Examples from the literature indicate that most supported transition-metal-oxide-based catalysts (Mo and V in particular) achieve ethylene yields in the range 15–30% (2, 5).

It is generally accepted that impregnation methods to support MoO_x over high-surface-area silica are limited by several factors such as choice of precursor and low reactivity of surface silanols (6). Thus, in the literature, detailed preparation methods were employed to enhance silica affinity for supported MoO_x species. Several methods were adopted such as increased concentration or reactivity of surface silanol groups, Mo complexes that directly react with the surface hydroxyl groups of silica, gas-phase grafting, nonaqueous impregnation, or sol–gel synthesis. Over the mixed oxides of silica and titania, a much better dispersion of MoO_x is obtained compared to that of the silica-supported catalyst. The addition of TiO_2 into the silica matrix has been shown to lead to unique structural and chemical properties that can provide advantages that the respective single oxides cannot (7–14). These benefits include stronger metal–support interactions, hindering both reduction and segregation of the active metal, and a smaller particle size that leads to a better dispersion and a higher surface area. Additionally, Klimova *et al.* (15) have achieved an enhanced dispersion of MoO_x over silica (MCM-41) by incorporating titania into the silica network. Much of these discussed properties are related to changes in surface acidity, porosity, Ti–O–Si connectivity, and phase segregations.

Gao *et al.* (16) prepared and characterized vanadium oxide species dispersed on TiO_2/SiO_2 (5–15 wt% TiO_2). Studies have shown that these catalysts are selective for the partial oxidation of ethane to ethylene due to the lower availability of oxygen atoms for total oxidation (17). The authors have concluded that the VO_x species preferentially interact with titanium oxide species. On the same samples, however, the addition of VO_x to TiO_2/SiO_2 was found to deplete some of the surface Si–OH hydroxyls, indicating that an interaction of VO_x with silica is not necessarily absent and that several supported species may be present with different $Ti–O^-$ and $Si–O^-$ ligands. This led the authors to describe the samples as bilayered surface metal oxide catalysts consisting of vanadium oxide and titanium oxide on silica. Research from the same laboratory (18) has reached the same conclusion for VO_x supported on Al_2O_3/SiO_2. Since the oxygenated ligands present around transition metal centers play a detrimental role in determining the reactivity of the surface species on mixed oxide supports, the characterization of both surface layers and support structures is crucial for understanding catalytic behavior.

In this work, a series of molybdena catalysts (0–20 wt% loadings) supported on mixed oxides of silica and titania were prepared by a "one-pot" sol–gel synthesis that distributes the molybdenum precursor through the Si : Ti support network as it forms. A review of the literature suggests that research on mixed oxides used as supports for active redox metal oxides has usually employed impregnation, incipient wetness, or grafting methods (19–24). A dispersed mixed oxide support is usually preformed to reach certain surface characteristics, such as dispersion or crystallinity. In our sol–gel method, we believe the one-pot preparation method can allow a greater possibility and a more even distribution of heterolinkages M–O–M′, where M and M′ can be Si, Ti, or Mo.

Prepared catalysts were studied with regard to their activity for the ODH of ethane. X-ray diffraction (XRD), Raman spectroscopy (ambient and dehydrated conditions), transmission electron microscopy (TEM), and X-ray photoelectron spectroscopy (XPS) were used to determine the nature of the molybdena species at various weight loadings. To demonstrate the structural differences obtained on a mixed oxide support, catalysts with single oxide supports of silica and titania were also prepared. Temperature-programmed desorption (TPD) was used to study changes in desorption behavior as a function of Mo wt% loading.

2. EXPERIMENTAL

2.1. Catalyst Preparation

Catalysts were prepared using a modified sol–gel/coprecipitation technique. Ammonium heptamolybdate (AHM) (Mallinkrodt) was used for the molybdenum precursor. For silica–titania mixed and single oxides, tetraethylorthosilicate (TEOS) (Aldrich) and titanium(IV) isopropoxide (TIPO) (Aldrich) were used. This method is referred to as a "one-pot" sol–gel/coprecipitation method and was described previously (25). In this modified sol–gel method, calculated amounts of the silica and titania alkoxide precursors were placed in a mixed alcohol solvent and hydrolyzed with the appropriate amount of an aqueous solution containing the Mo precursor. The added aqueous solution contained the stoichiometric amount of water necessary to hydrolyze all of the alkoxide precursors. Synthesized catalysts are listed in Table 1. Catalysts numbered 1

TABLE 1

Sol–Gel Prepared Catalysts

Catalyst no.	Composition	Surface area (m^2/g)
1	Si : Ti 1 : 1	320
2	2% Mo/Si : Ti 1 : 1	343
3	5% Mo/Si : Ti 1 : 1	246
4	10% Mo/Si : Ti 1 : 1	210
5	15% Mo/Si : Ti 1 : 1	188
6	20% Mo/Si : Ti 1 : 1	116
7	10% Mo/SiO_2	548
8	10% Mo/TiO_2	91

through 6 are a series of Si : Ti 1 : 1 supported Mo catalysts (0–20 wt%). Catalysts 7 and 8 are 10 wt% loading of Mo over SiO_2 and TiO_2, respectively. For comparison purposes, pure oxides of both silica and titania were also prepared by the same method.

2.2. Catalyst Characterization

BET surface-area measurements and nitrogen adsorption–desorption isotherms were recorded using a Micromeritics AccuSorb 2100E instrument. X-ray diffraction patterns were obtained with a Scintag PAD-V diffractometer using Cu$K\alpha$ radiation. TEM images and quantitative elemental analyses were performed on a Philips CM-300 FEG microscope equipped with a light element EDS X-ray detector. Raman spectra were recorded with a Dilor spectrometer using the 514.5-nm line of an Innova 300 Ar laser. Spectra were taken in the range 200–1800 cm^{-1} in a 180° back-scattering mode with a Spectrum One CCD detector. Raman spectroscopy was performed under dehydrated conditions using a quartz *in situ* flow cell that was capable of bringing the catalysts in contact with a gas flow at high temperatures. A portion of the prepared samples were recalcined at 550°C for 30 min under pure O_2 and transferred into the Raman cell. Additional dehydration occurred at 350°C for 30 min under a flow of dry 10% O_2/He after which the cell was sealed. Spectra were taken under 10% O_2/He atmosphere at room temperature. Thermogravimetric analysis was performed with a Perkin–Elmer TGA 7 thermogravimetric analyzer. Samples were pretreated in dry air at 500°C for 30 min before analysis. The weight loss of ambient-exposed samples (50 mg) versus temperature was recorded under a dry helium flow of 30 cm^3/min. The differential weight-loss curves (DTG) were analyzed with the accompanying Perkin–Elmer software package. The temperature program was as follows: 10 min at 30°C, 5°/min ramp rate to 800°C and 15 min at 800°C.

X-ray photoelectron spectroscopy was performed using an ESCALAB MKII ESCA/Auger spectrometer operated at 14 kV and 20 mA using Mg$K\alpha$ radiation. Spectra were corrected using the C1*s* signal, located at 284.6 eV. Surface concentrations were determined using instrumental atomic sensitivity factors.

Ethane temperature programmed desorption was performed using a laboratory-made gas flow system described elsewhere (26). Catalyst samples (150 mg) were placed in a 1/4-in.-i.d. U-tube quartz reactor, pretreated under oxygen flow at 550°C for 30 min, then cooled to room temperature under helium, and finally flushed with helium for 1 h following 1 h of propane adsorption. Species desorbing under a helium carrier gas were monitored by a mass spectrometer (HP5890GC-MS). For these studies, the GC columns were replaced by an empty capillary column. The mass spectrometer was equipped with a quadrupole mass analyzer that allows tracking of up to 20 mass-to-charge ratios (m/z) simultaneously in the selected ion mode. The identification of species with equal m/z ratios was accomplished by following characteristic mass fragments of the species. The temperature program was as follows: 10 min at room temperature, 10°/min ramp rate to 800°C, and 10 min at 800°C.

2.3. Oxidative Dehydrogenation of Ethane

Steady-state reaction experiments were carried out in a fixed-bed, quartz reactor, operated at ambient pressure. A HP 5890 series II gas chromatograph equipped with FID and TCD detectors performed separations and analyses of reaction products online. Separations were performed using three columns: (1) Hayesep D (8 ft × 1/8 in.) for hydrocarbons and partially oxygenated hydrocarbons, (2) Porapak Q (6 ft × 1/8 in.), and (3) molecular sieve 5 Å (6 ft × 1/8 in.) for N_2, O_2, CO, CO_2, and H_2O. Catalyst samples, ranging from 0.1 to 1.5 g, were held in place by a quartz frit. The feed consisted of ethane/oxygen/nitrogen at a flow rate of 25 cm^3/min. The amount of nitrogen and the ethane/oxygen ratio were varied for some runs. The concentration of the feed stream was maintained outside the flammability limits of ethane–oxygen–nitrogen mixtures for all runs. The main products of the dehydrogenation reaction were ethylene, methane, carbon dioxide, carbon monoxide, and water. Acetaldehyde was only observed to form over 10% Mo/SiO_2. The product distributions maintained a carbon balance of 100% (±5%) except for 10% Mo/SiO_2 due to inadequate separation/quantification of acetaldehyde from water.

For the oxidative dehydrogenation of ethane, the contribution of homogeneous reactions due to ethyl radicals formed at the surface and desorbed into the gas phase can be significant. Thus, it is necessary to distinguish catalytic activity from gas-phase activity in order to study the effectiveness of the catalysts. Burch and Crabb have studied homogenous contributions to the catalytic ODH of ethane and have confirmed that filling the dead space of the reactor with quartz inhibits gas-phase radical reactions (27). To ensure that the homogenous reaction is indeed eliminated by this technique, reaction tests were run using an empty-volume quartz reactor. The results of this experiment showed no conversion of ethane up to 650°C under the feed conditions studied. During catalytic reaction experiments, the dead volume of the quartz reactor was packed with quartz wool and ceramic beads to minimize any gas-phase effects that might occur in the presence of a catalyst.

3. RESULTS AND DISCUSSION

3.1. Catalyst Characterization

From 2 through 20 wt% loading of molybdena, the catalysts showed a general decrease in surface area with increasing amounts of molybdenum added. X-ray diffraction

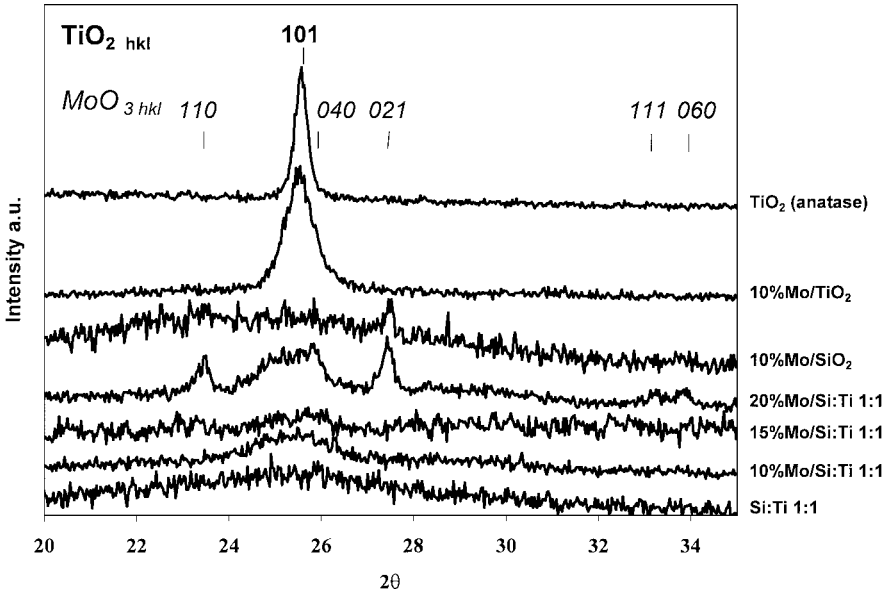

FIG. 1. X-ray diffraction patterns of Mo/Si : Ti catalysts with different Mo wt% loadings.

patterns of the Mo wt% loaded catalysts are shown in Fig. 1. X-ray diffraction of the Si : Ti 1 : 1 support yielded a pattern characteristic of a silica–titania mixed oxide (28). One broad peak with a center located at a *d* spacing of 3.59 Å was observed, which is indicative of a finely dispersed, small X-ray particulate anatase structure supported over amorphous silica. For comparison, the X-ray diffraction pattern of TiO_2 (anatase structure) is included in the figure. When molybdenum is added, this peak becomes narrower, indicating a change in the dispersion and segregation of titania in the Si : Ti matrix with the addition of Mo. None of the samples showed any indication of a rutile phase. On images obtained with TEM over the Si : Ti support, an average 2-nm particle size was observed with evidence of crystalline TiO_2 homogeneously distributed throughout the sample. However, with the addition of molybdenum to the Si : Ti 1 : 1 support, the larger size of TiO_x domains in the sample was more readily observed as indicated by the lattice fringes from crystalline TiO_2. These lattice fringes, with an average spacing of ~3.3 Å, were more prominent than those in the Si : Ti 1 : 1 support (29). Molybdena species are finely dispersed showing no MoO_3 diffraction lines up to 15 wt% loading on the mixed oxide support. However, it may be possible for MoO_3 to exist as a microcrystalline material below the XRD detection limit. Features from crystalline MoO_3 become detectable when the Mo loading level is increased to 20 wt%. For 10 wt% Mo on silica, only one peak associated with the (021) plane of crystalline MoO_3 is resolved. For 10 wt% Mo on titania, no feature associated with crystalline MoO_3 is detected. It is interesting to note that, although the surface area of the silica-supported sample is much larger than that of Mo/TiO_2, the titania support appears to provide a better dispersion of the metal oxide.

Raman spectra were recorded under ambient and dehydrated conditions for catalysts with different Mo loadings as well as for the Si : Ti 1 : 1 support. Figure 2 shows the change in the Raman spectra (focused on the range 540–1040 cm^{-1}) when the Si : Ti 1 : 1 support is dehydrated. For comparison, Raman spectra (ambient and dehydrated) of pure silica are also included. The dehydrated Si : Ti 1 : 1 surfaces have Raman bands at 605, 800, 916, and 1080 cm^{-1}. The

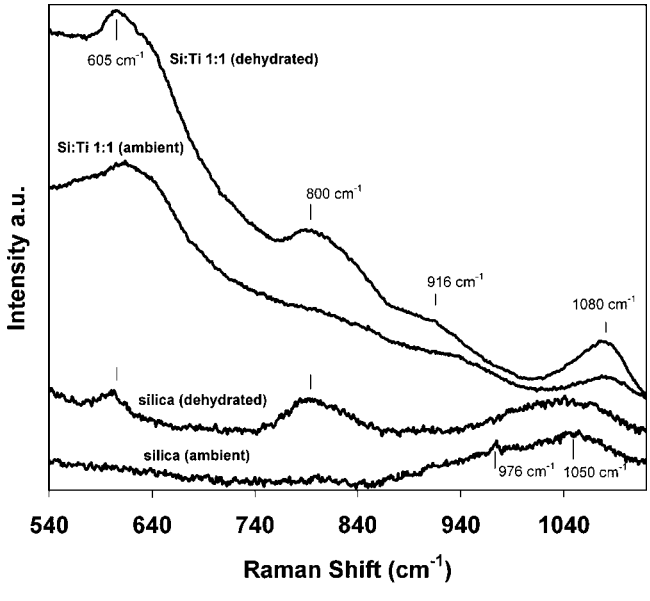

FIG. 2. Raman spectra of Si : Ti 1 : 1 support under ambient and dehydrated conditions.

band at 605 cm^{-1} is assigned to tricyclosiloxane rings of the silica produced via the condensation of surface hydroxyls upon dehydration, while the band at 800 cm^{-1} is attributed to the symmetric mode of Si–O–Si stretching (30). On pure silica, a distinct band can be observed at 976 cm^{-1} under ambient conditions. This band is ascribed to surface silanols and is seen to disappear upon dehydration of the sample. In the literature, the bands located at 916 and 1080 cm^{-1} have been assigned to perturbed silica vibrations that are indicative of Ti–O–Si bonds (30–32). However, the broad band at 1080 cm^{-1} can be convoluted with the expected asymmetric mode of Si–O–Si stretching at ~1050 cm^{-1} (33). When compared to silica, the 1050-cm^{-1} band can be seen to sharpen and shift to 1080 cm^{-1}. An important feature of these spectra is the dispersed nature of TiO_x species. The most intense Raman band from TiO_2 (anatase) can be seen only as a weak and broad shoulder located around 640 cm^{-1}.

Thermogravimetric analysis of the SiO_2, TiO_2, and Si : Ti 1 : 1 supports reveals that all physically adsorbed water leaves the supports between 150 and 200°C. An analysis of the DTG curves can show the temperature at which dehydroxylation begins and thus give insight as to the origin (i.e., TiO_2 or SiO_2) and thermal stability of chemically bound hydroxyl groups. The dehydroxylation was found to occur in a single-step process beginning at a single temperature (TiO_2, 303°C; SiO_2, 325°C; Si : Ti 1 : 1, 325°C) as summarized in Fig. 3. The concentration of hydroxyls was calculated based on the surface area of the samples and the total weight loss after dehydroxylation begins. The temperature of dehydroxylation is the same for SiO_2 and Si : Ti 1 : 1. This, together with the fact that there was no lower temperature peak observed in the DTG curve which might correspond to hydroxyls on titania, suggests that the hydroxyls on Si : Ti are largely from silica. Furthermore, there is no significant change in the strength of hydrogen bonding of clustered hydrolyzed Si–OH---HO–Si bonds since the temperature of dehydroxylation (Si–OH---HO–Si → Si–O–Si + H_2O) for pure SiO_2 is roughly the same as that for the Si : Ti 1 : 1. Quaranta *et al.* (34) have found that, on TiO_2/SiO_2 samples prepared by homogeneous precipitation, a substantial amount of the silica surface remains uncovered even above monolayer coverage. Furthermore, Armaroli *et al.* (32) have suggested that in TiO_2/SiO_2 aerogels of up to 40 wt% TiO_2, silica tends to form an overlayer on a TiO_2 core and the surface is dominated by silanol groups similar to those of pure silica. The authors, through IR studies of adsorbed acetonitrile, detected no increase in the acidity (strength) of the surface silanols after incorporation of titania to silica.

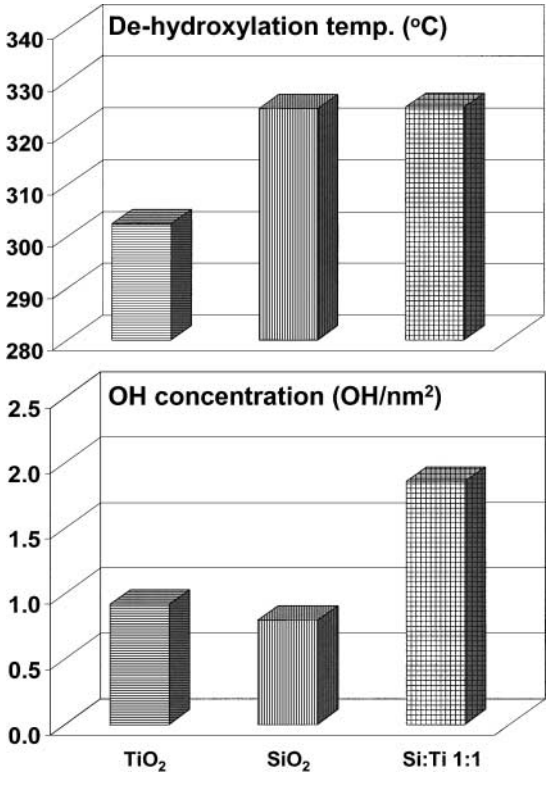

FIG. 3. Dehydroxylation temperatures and hydroxyl concentrations of support materials as determined by TGA analysis.

Compared to either SiO_2 or TiO_2, the overall concentration of hydroxyls is increased in Si : Ti 1 : 1 (Fig. 3). Since the hydroxyl concentrations, based on surface areas of SiO_2 and TiO_2 are almost equal, the possibility of hydroxyls associated with TiO_x species in Si : Ti 1 : 1 cannot be completely ruled out, even though Ti–OH species were not detected in the TG analysis of the Si : Ti 1 : 1 support. For a pure titania support, it has been previously shown that the preparation of a high-surface-area titania of small particle size, such as that obtained from sol–gel methods, can alter surface acidity and lead to several types of surface hydroxyls (35). Nonetheless, Si : Ti 1 : 1 was found to have an increased hydroxyl concentration compared to that of SiO_2, which can conceivably arise from the perturbation of the surface by Ti–O–Si interactions.

The Raman spectra of 10 wt% Mo catalysts supported on TiO_2 and SiO_2 are shown in Fig. 4 (ambient and dehydrated conditions). These samples are prepared in the same manner as the catalysts which are supported on the mixed oxide Si : Ti. Bands arising from poorly dispersed crystalline MoO_3 are present over the SiO_2-supported catalysts at 671, 820, and 996 cm^{-1} and do not change upon dehydration. Small bands, located at 781, 854, 877, and 957 cm^{-1} that are assigned to MoO_x species in polymolybdate structures (6) are present in the ambient Raman spectra but disappear upon dehydration. In general, bands in the range 750–950 cm^{-1} are attributed to antisymmetric stretching of Mo–O–Mo bonds or symmetric stretching of $(-O-Mo-O-)_n$ bonds, while bands in the range 950–1050 cm^{-1} can be attributed to the stretching of Mo=O bonds (36). In particular, the broad Mo=O band at 957 cm^{-1} can be assigned to both $Mo_8O_{26}^{4-}$ and $Mo_7O_{24}^{6-}$

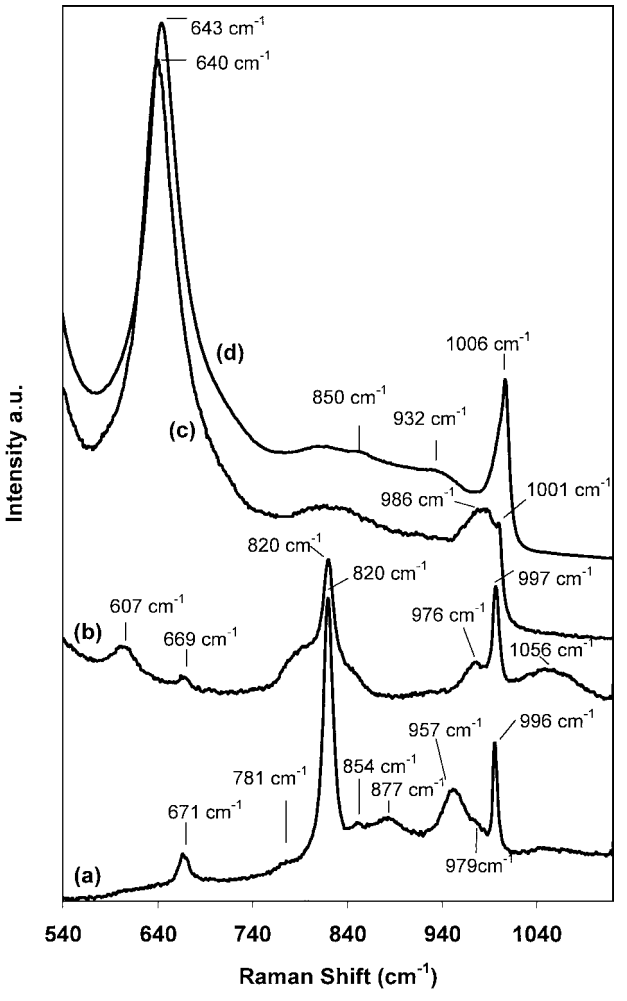

FIG. 4. Raman spectra of 10% Mo/SiO_2. (a) Ambient conditions, (b) dehydrated conditions and 10% Mo/TiO_2, (c) ambient conditions, (d) dehydrated conditions. Spectra taken under 10% O_2/He at room temperature.

polymolybdate species (6, 37). In the Raman spectra of 10% Mo/SiO_2 before and after dehydration, a distinct band at 976–979 cm^{-1}, which could be assigned to Mo–O–Si surface bonds (6, 38), is present. However, a Raman band of surface silanols is also reported to occur at around 970–976 cm^{-1} (28, 39). Also, the bands that are typical of the SiO_2 support (607, 800, and 1050 cm^{-1}) are visible in the spectrum taken from the dehydrated sample.

For 10% Mo/TiO_2, no crystalline MoO_3 is observed, and a band arising from surface-supported MoO_x appears at 1001 cm^{-1} that shifts to 1006 cm^{-1} and becomes more intense upon dehydration. Furthermore, there is a broad feature at 986 cm^{-1} that completely disappears upon dehydration. However, bands arising from polymolybdate species become slightly more visible (850 and 932 cm^{-1}) when 10% Mo/TiO_2 is dehydrated. The results indicate significant differences in the way titania and silica can support MoO_x. The segregation of crystalline MoO_x over silica is commonly observed and arises from the low reactivity of the surface hydroxyls of silica toward MoO_x, causing the formation of bulk MoO_3 crystallites (40, 41). However, a more intriguing difference is the change of bands arising from molybdenum poly-oxo structures upon dehydration. Over the silica-supported sample, these bands disappear, while over titania, bands at 850 and 932 cm^{-1} become more pronounced as the broad band at 986 cm^{-1} disappears. In the literature, several researchers have observed the disappearance of polymolybdate bands over Mo/SiO_2 catalysts upon dehydration. Furthermore, hydration can result in the hydrolysis of Mo–O–Si bonds to create surface hydroxyls. Upon dehydration, these hydroxyls reinteract with the surface MoO_x species (42). It appears that titania is able to accommodate stable poly-oxo molybdenum species, while silica supports only a small amount of MoO_x species since MoO_x is largely present as crystalline MoO_3.

Figure 5 shows the Raman spectra of ambient-exposed Mo/Si : Ti 1 : 1 catalysts covering the Mo=O and Mo–O–Mo vibrational frequency ranges, together with the most intense Raman band from TiO_2 (anatase) 632–640 cm^{-1}. An important feature of these spectra is that there is no evidence of crystalline MoO_3 up to 15 wt% loading. At 20 wt% loading, formation of crystalline MoO_3 is apparent by the bands located at 663, 819, and 996 cm^{-1}. The broad bands associated with isolated terminal Mo=O stretching vibrations were observed to shift with Mo wt% loading from 973 cm^{-1} at 2 wt% to a maximum of 998 cm^{-1} at 15 wt%. Shifts in the Mo=O Raman frequency are related to changes in bond length (37) and can be ascribed to a decreasing interaction with the support and the formation of three-dimensional structures. The Raman band of TiO_2 is observed in all samples (640 cm^{-1}), except in 2% Mo/Si : Ti 1 : 1 where it has shifted to 632 cm^{-1}. This feature indicates that TiO_x is

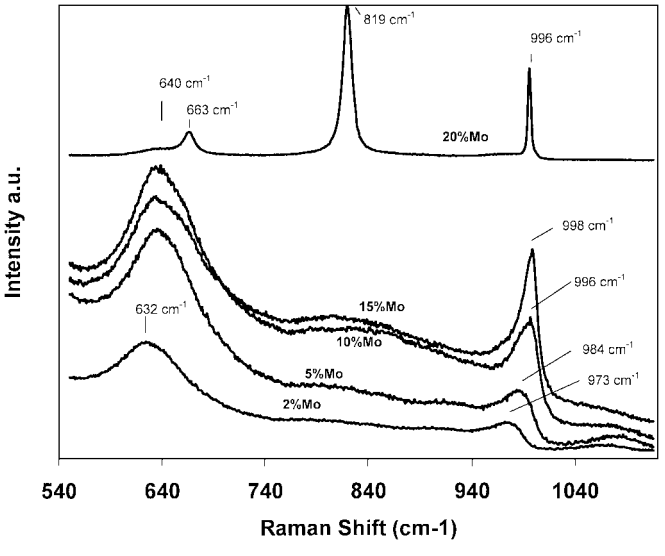

FIG. 5. Raman spectra (ambient conditions) of Mo/Si : Ti 1 : 1 catalyst with different Mo wt% loadings.

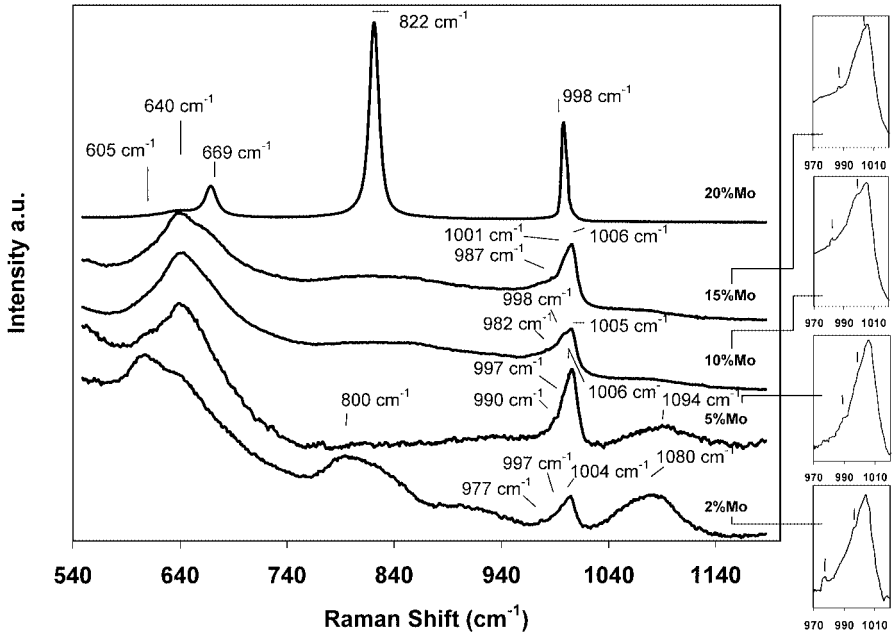

FIG. 6. Raman spectra (dehydrated conditions) of Mo/Si : Ti 1 : 1 catalyst with different Mo wt% loadings. Spectra taken under 10% O_2/He at room temperature.

well dispersed on this sample, whereas with increasing wt% loading of molybdenum, larger domains of TiO_2 (anatase) are readily formed.

A pronounced change is observed in the Raman spectra of Mo/Si : Ti 1 : 1 catalysts under dehydrated conditions (Fig. 6). Perhaps the most important feature is that the isolated terminal Mo=O stretching vibrations shift to higher wavenumbers for all samples, and several shoulders can be observed in the broad vibration. At the same time, changes in the silica network with Mo wt% loading can be readily observed. As under ambient conditions, there is no evidence of crystalline MoO_3 up to 15 wt% loading. The main Mo=O Raman frequency remains essentially unchanged with wt% loading (1004–1006 cm^{-1}) until crystalline MoO_3 appears at 20 wt%. Small, yet discernible, shoulders are observed in the main Mo=O Raman band for 2 wt% loading at 977 and 997 cm^{-1}. With increased wt% loading, the shoulder at 977 cm^{-1} is no longer observed, while higher wavenumber shoulders are still observed up to 15 wt% (5 wt% Mo, 990 cm^{-1}; 997 cm^{-1}; 10 wt% Mo, 982, 998 cm^{-1}; 15 wt% Mo, 987, 1001 cm^{-1}). The band present on 2% Mo/Si : Ti 1 : 1 at 977 cm^{-1}, as stated previously, could arise from Si–O–Mo bonds corresponding to a silicomolybdic acid species.

An examination of the bands from the Si : Ti 1 : 1 support present in the Raman spectra of Mo/Si : Ti 1 : 1 catalysts under dehydrated conditions reveals changes with molybdenum wt% loading that are not resolved under ambient conditions. On 2% Mo/Si : Ti 1 : 1, bands are present from the silica support at 605 and 800 cm^{-1}, from TiO_2 (anatase) at 640 cm^{-1}, and from Si–O–Si and/or Si–O–Ti bonds centered at ~1080 cm^{-1}. In general, the features from the silica support are decreasing with Mo wt% loading. The silica bands at 605 cm^{-1} are seen to decrease with 5 wt% loading and become unresolved at 10 wt% loading. The band at ~1080 cm^{-1} shows the same trend. The broad band at 800 cm^{-1} disappears altogether at 5 wt% loading. This could be an indication that, as Mo wt% loading is increased, there is increased coverage of the silica on the support. Concurrent with these trends is a relative increase in the TiO_2 band at 640 cm^{-1}.

A question arises as to whether it can be established if MoO_x species are preferentially supported over SiO_x or TiO_x domains, and if so, to what extent. Wachs (37) has summarized the Raman spectroscopy results for Mo/SiO_2 and Mo/TiO_2 prepared by several methods and stated that Mo=O Raman bands of surface-supported MoO_x on titania appear in the range 998–1001 cm^{-1}. On silica, these bands are reported to be a function of wt% loading and appear in the range 975–990 cm^{-1}. Considering the results in this context, MoO_x species attached to titania (Raman bands present 1004–1006 cm^{-1}) and species attached to silica (Raman bands present as shoulders in the range 977–998 cm^{-1}) appear to coexist. However, Gao *et al.* (16) describe the $VO_x/TiO_2/SiO_2$ (5–15 wt% TiO_2) system as a bilayered surface metal oxide catalyst consisting of vanadium oxide and titanium oxide on silica with several supported species containing different Ti–O^- and Si–O^- ligands. While the extent of the MoO_x interaction with each component of the Si : Ti 1 : 1 support cannot be determined from the Raman spectra, considering the similarity of the

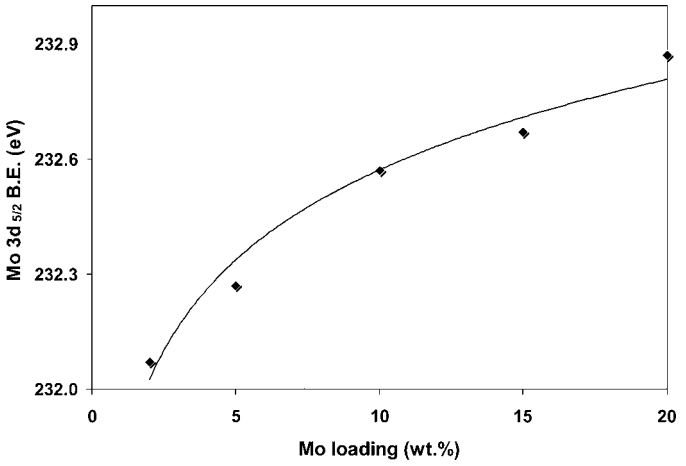

FIG. 7. Variation in Mo $3d_{5/2}$ BE of Mo/Si : Ti 1 : 1 catalysts with different Mo wt% loadings.

spectrum of 10% Mo/TiO_2 to that of the Si : Ti 1 : 1 supported catalyst, it would appear that more MoO_x species are supported on titania. However, the decrease in the Raman bands of silica observed with increasing wt% loading seems to suggest an increased interaction of MoO_x with silica, possibly leading to perturbation of the Si–O–Si matrix or even formation of Si–O–Mo linkages.

To further study the dispersion of MoO_x over the Si : Ti 1 : 1 support, XPS was performed over samples with various Mo wt% loadings. XPS (Mo3*d* region) of Si : Ti 1 : 1 supported catalysts exhibited one linked doublet corresponding to Mo$3d_{5/2}$ and $3d_{3/2}$ binding energies. The variation in molybdenum $3d_{5/2}$ binding energies with Mo wt% loading over Si : Ti 1 : 1 is shown in Fig. 7. The binding energy is seen to shift from 232.0 eV (2 wt% Mo) to 232.9 eV (20 wt% Mo) approaching that of bulk MoO_3 (Mo $3d_{5/2}$ BE = 233.4 eV). An additional feature (Mo $3d_{5/2}$ BE = 229.1 eV) was observed within the spectrum of the 2% Mo/Si : Ti 1 : 1 catalyst. This lower BE feature was ascribed to the presence of Mo–O–Si bonds (42) and is not present in the spectra of the catalysts with higher wt% loading.

Additional XPS characterization (Si2*p*, Ti2*p*, and O1*s*) is shown in Fig. 8. The Ti$2p_{3/2}$ binding energy (Fig. 8a) is seen shifting to lower values with increasing Mo wt% loading, from 459.2 eV for the Si : Ti 1 : 1 support to 458.3 eV for 20 wt% Mo. The Ti$2p_{3/2}$ binding energy of pure anatase is around 458.0 eV. There is also a pronounced feature in the Ti2*p* spectrum of the Si : Ti support located at 456.5 eV. Although less pronounced, this feature is seen in the spectrum of 2% Mo/Si : Ti 1 : 1. This feature may be associated with Ti atoms present in Ti–O–Si. Fernandez *et al.* (43) have assigned an XPS feature at 456.4 eV to a reduced titania site (Ti^{3+}). While this remains a possibility, it is more likely that the Ti site responsible for the XPS feature in Fig. 8a may be an electron-rich species produced by the integration of Ti into the silica network at boundaries and not a fully reduced site. Notari (44) points out that in TiO_2-rich samples of Si : Ti, the Ti^{4+} in Ti–O–Si shares negative charges more from the oxygen in SiO_2 than from the oxygen of the bulk. The large difference between the BE of the pure anatase phase and that of the Si : Ti support are indicative of TiO_x closely interacting with the silica surface (38). The fact that the difference becomes smaller; i.e., that the BE of the catalyst approaches that of pure anatase with increasing Mo wt% loading, suggests that the presence of Mo may be interfering with the Si–Ti interaction, as will be further discussed. The Ti/Si surface atomic ratio, as determined from

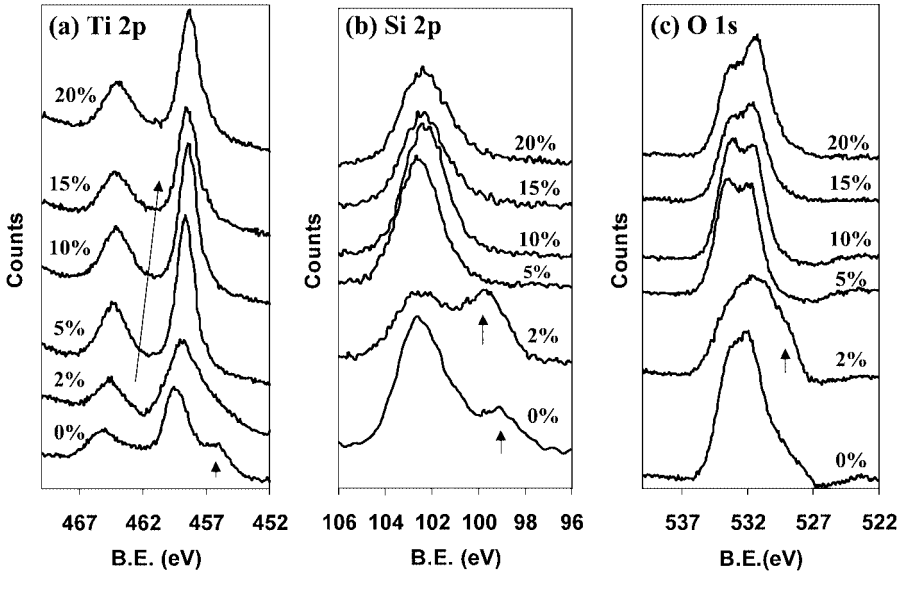

FIG. 8. XPS spectra of Mo/Si : Ti 1 : 1 catalysts with different Mo wt% loadings. (a) Ti $2p_{3/2}$, (b) Si 2*p*, (c) O 1*s*.

XPS, indicates that there is less Ti at the surface (Ti/Si = 0.6–0.4 for all catalysts) than in the bulk (Ti/Si = 1). This indicates that silica is preferentially concentrated at the top layers (10–50 Å) of the surface.

The Si2*p* XPS spectra (Fig. 8b) show a peak, located at ~102.3 eV, characteristic of SiO_2. There is an additional feature in the Si2*p* spectra of the Si : Ti 1 : 1 support and the 2% Mo/Si : Ti 1 : 1 sample. For the Si : Ti support, there is a shoulder present at ~99.0 eV. This feature is assigned to the Si atoms of Ti–O–Si. Additionally, there is a shoulder present in the spectrum of 2% Mo/Si : Ti 1 : 1, BE ~99.8 eV. Because only a weak signal from Si–O–Ti was detected in the Ti2*p* spectrum of the 2 wt% loading sample, this pronounced change is likely due to another species and can be considered as further evidence of a Mo–O–Si species. The O 1s XPS spectra, shown in Fig. 8c, reveal oxygen contributions from TiO_x, SiO_x, and MoO_x. The O 1s spectrum of SiO_x is located at ~533.4 eV, while the signals from TiO_x and MoO_x coincide at around 530 eV. Furthermore, there is evidence of Si–O–Ti species, which can exhibit an O 1*s* band in between those of SiO_2 and TiO_2, making the peak significantly broadened. The O 1s spectrum of 2% Mo/Si : Ti 1 : 1 appears substantially different from that of the Si : Ti support. Again, it appears that, there is an additional feature present in the spectrum for 2% Mo/Si : Ti 1 : 1 located at ~527 eV that could be ascribed to the same Mo–O–Si interaction species.

The surface concentrations, as determined by XPS, are shown in Fig. 9. As expected, there is an increase in Mo surface concentration with wt% loading that approximately corresponds to the bulk percentage. At the lowest wt% loading studied, 2 wt%, the percentage of Ti at the surface decreases, while that of silica increases compared to that of bare Si : Ti 1 : 1. This could indicate that low loadings of MoO_x preferentially cover TiO_x domains. However, as Mo wt% loading increases, the surface concentration of Ti remains constant. On the other hand, the change in the Si surface concentration exhibits a mirror image of the change in the Mo surface concentration, where the increase in one is accompanied by an equal decrease in the other. Reddy *et al.* (46) have used XPS to quantify Mo dispersion on their 12 wt% Mo samples supported on various mixed oxides with ratios of 1 : 1 (Si, Ti, Zr, and Al). XPS surface compositions indicated that MoO_x is more dispersed on SiO_2 than on TiO_2 over the Si : Ti 1 : 1 support. However, the dispersion of MoO_x, characterized in this manner, depends on the surface concentrations of the mixed oxides before molybdenum incorporation (i.e., the Si and Ti content before introduction of MoO_x). In our study, the data suggest that MoO_x is supported on both silica and titania domains with an increasing affinity for silica as loading is increased from 2 to 15 wt%. This is in agreement with the Raman spectroscopy results presented. Raman data indicate that MoO_x is supported preferentially on titania; however, the interaction with silica, present even at the lowest wt% loading, increases with the wt% loading of molybdenum until the formation of crystalline MoO_3 occurs. The Raman data also suggest that poly-oxo molybdenum species may be more stable on titania than on silica. Thus, it is plausible that there are significant structural differences in the MoO_x species supported on silica versus titania and that these differences may give rise to the observed differences in surface compositions.

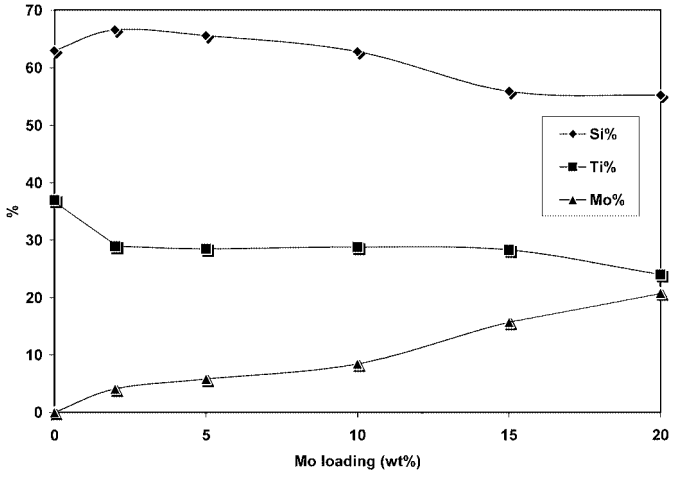

FIG. 9. Variation of Mo/Si : Ti 1 : 1 surface concentrations (XPS) with Mo wt% loading.

However, it has been stated (7) that Ti atoms in TiO_2/SiO_2 may be located inside either channels or pores of silica that may be out of the range of XPS. Thus, it may be possible that in this "one-pot" preparation method, in which components are dispersed together during gelation, all the MoO_x and TiO_x species may not be preferentially located at the surface. Furthermore, there may be a significant amount of molybdena species located either inside larger titania aggregates or deeper inside the silica network. Combined with the fact that MoO_x species may share several types of support ligands with differing electronegativity, it seems inadequate to describe MoO_x species as being supported exclusively on either SiO_2 or TiO_2 domains. The presented results indicate that, with this preparation method, Mo wt% loading not only affects the structure of the surface MoO_x species but also influences the nature of TiO_x/MoO_x concentrations over the silica. As molybdenum loading is increased, there is a greater degree of crystalline titania segregation. At the same time, there appears to be an increased interaction of the silica with MoO_x.

3.2. Reaction Experiments for the Oxidative Dehydrogenation of Ethane

Mo/Si : Ti catalysts were compared in the ODH reaction using equal-surface-area loading (200 m^2) in the reactor at temperatures of 550 and 600°C. The feed percentages for

TABLE 2

Ethane ODH Reaction Data—Support Comparison

Catalyst	Temperature (°C)	Conversion (%) C_2H_6	Selectivity (%) C_2H_4	CO_2	CO	CH_4
Si : Ti 1 : 1	550	5.1	41.2	58.6	0.0	0.2
	600	6.0	51.7	48.1	0.0	0.2
10% Mo/SiO_2	550	5.1	49.6	12.1	38.3	0.0
	600[a]	21.0	31.7	11.3	34.1	0.6
10% Mo/TiO_2	550	25.8	38.5	19.5	38.9	3.1
	600	33.6	47.9	15.8	32.3	4.0
10% Mo/Si : Ti 1 : 1	550	29.3	39.3	19.0	30.4	12.6
	600	39.2	44.1	17.8	12.3	28.8

[a] Acetaldehyde formation observed.

these experiments were $N_2/C_2/O_2$: 85/10/5. Reaction data were taken after steady state was reached.

The influence of support composition on catalytic performance is shown in Table 2 and Fig. 10. By comparing the performance of Si : Ti 1 : 1, TiO_2, and SiO_2 supports for 10 wt% loading, we see that the titania-supported catalyst behaves quite similarly to that supported on Si : Ti 1 : 1 at both 550 and 600°C. However, the titania-supported catalyst, when compared to the Si : Ti 1 : 1 support, shows an increased selectivity to carbon monoxide and a decreased selectivity to methane. At 550°C, the SiO_2-supported catalyst exhibits an ethane conversion much lower than that of the TiO_2-supported catalyst. A similar difference in activity, although less pronounced, is also observed at 600°C. The Raman spectra of 10% Mo/SiO_2 indicates that MoO_x is largely present as crystalline MoO_3 with only slight evidence for surface-supported species. This could possibly explain the very different reaction behavior of this catalyst. Acetaldehyde was observed to form in an appreciable amount over 10% Mo/SiO_2 at 600°C. Banares (47) has stated in a recent review that water vapor are essential for acetaldehyde formation over MoO_x/SiO_x from ethane/oxygen reactants and that surface molybdenum oxide species interacting with silica are active in acetaldehyde formation. Acetaldehyde formation could possibly result from a surface reaction involving adsorbed water (as −OH) or oxygen that could easily be formed on the high-surface-area silica. However, further characterization would be needed to make a distinction.

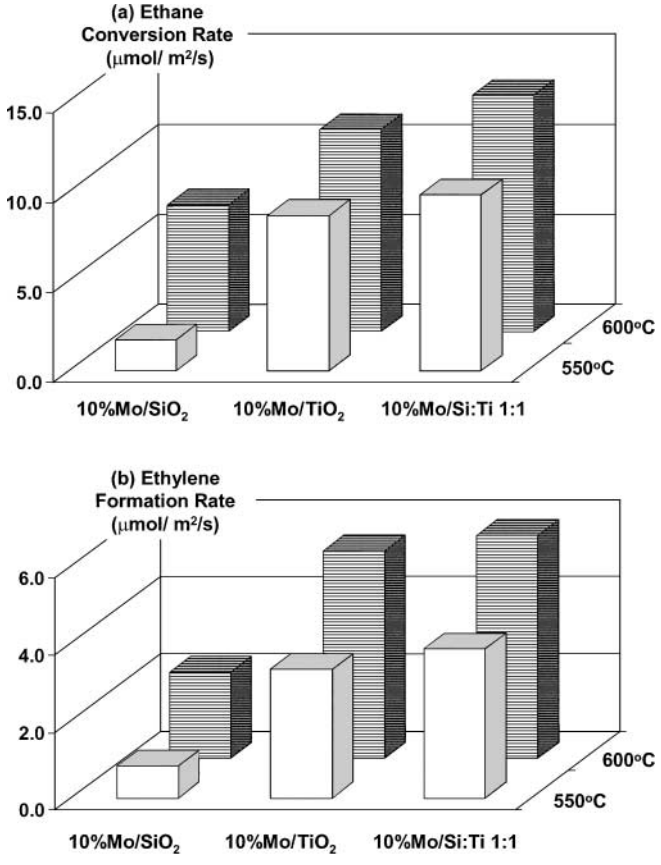

FIG. 10. Comparison of support materials for 10 wt% Mo loading. (a) Ethane conversion rates and (b) ethylene formation rates for equal-surface-area (~200 m^2) reaction experiments (μmol/m^2/s).

As the Raman spectra and XRD patterns indicate, the surface-supported species over titania and Si : Ti 1 : 1 are rather similar, while those on SiO_2 are quite different. It is generally accepted that surface metal oxide species primarily anchor to the support by "titration" of the surface hydroxyl sites (37). As previously mentioned, silica is unable to stabilize large amounts of supported MoO_x species, even well below monolayer coverage, and crystalline MoO_3 segregation occurs. However, titania has been shown to disperse Mo much more effectively than silica (48). Therefore it is conceivable that MoO_x is supported over pure TiO_2 in a well-dispersed manner.

When the performances in ethane ODH at different Mo wt% loadings (Table 3) are compared, reaction data indicate that ethane conversion increases to a maximum

TABLE 3

Ethane ODH Reaction Data—Mo Wt% Loading Comparison

Catalyst	Temperature (°C)	Conversion (%) C_2H_6	Selectivity (%) C_2H_4	CO_2	CO	CH_4
2% Mo/Si : Ti 1 : 1	550	20.9	38.3	40.9	20.4	0.8
	600	27.6	36.7	37.9	19.4	6.1
5% Mo/Si : Ti 1 : 1	550	26.8	40.1	14.3	39.8	5.9
	600	37.0	34.9	12.9	25.0	26.8
10% Mo/Si : Ti 1 : 1	550	29.3	39.3	19.0	30.4	12.6
	600	39.2	44.1	17.8	12.3	28.8
15% Mo/Si : Ti 1 : 1	550	30.1	34.4	19.4	43.3	1.0
	600	43.8	26.5	20.7	42.7	9.4
20% Mo/Si : Ti 1 : 1	550	24.5	33.8	32.4	30.1	3.7
	600	31.9	34.3	32.5	22.0	11.2

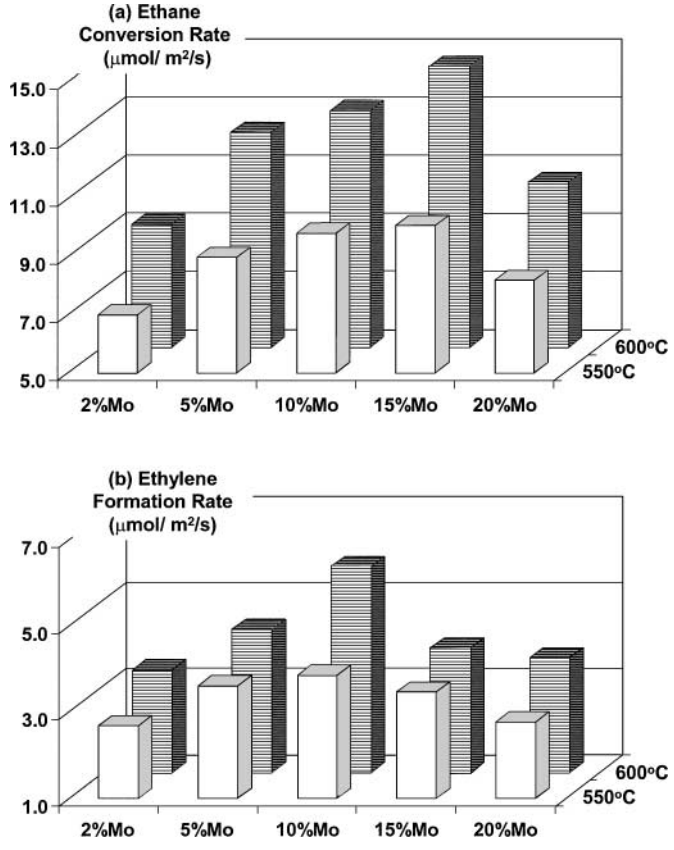

FIG. 11. Comparison of Mo/Si : Ti 1 : 1 catalysts to different Mo wt% loadings. (a) Ethane conversion rates and (b) formation rates for equal-surface-area (~200 m^2) reaction experiments (μmol/m^2/s).

at 15 wt% Mo at both 550 and 600°C declining at 20 wt% Mo. The ethylene yield increased to a maximum at 10% Mo/Si : Ti 1 : 1 giving 11.5, and 17.3% at 500 and 600°C, respectively. The trend in ethane conversion and ethylene formation, normalized to catalyst surface area, is illustrated in Fig. 11. It is found that normalized ethylene formation reached a maximum at a Mo loading level of 10 wt% at both temperatures studied. It is important to note that increased ethylene yields are accompanied by an increase in methane selectivity for these reaction conditions. This may possibly be a contribution from the surface-assisted pyrolysis of ethane or ethlyene, which is reported to occur at temperatures as low as 500°C (49), even though no ethane conversion was detected in blank reactor experiments up to 600°C. It is less likely, but also possible, that a mechanism exists for methane formation to take place from the decomposition of an ethoxide or other oxygenated surface intermediate.

The Raman spectra of Mo/Si : Ti 1 : 1 catalysts taken under ambient conditions have shown that terminal Mo=O stretching vibration shifts to a higher wavenumber with increasing Mo wt% loading (42). Chen *et al.* (50) have related a similar increase in the Mo=O Raman frequency (ambient conditions) of supported MoO_x to a decrease in propane ODH reactivity over Mo/ZrO_2 catalysts. Here, the propane conversion rate, normalized per Mo atom, decreased steadily with increasing MoO_x wt% loading over ZrO_2. However, this trend seems highly dependent on the support, as research from the same laboratory (51) has shown that the propane conversion rate, normalized per Mo atom, went through a maximum at intermediate MoO_x loading over Al_2O_3. The difference is likely to arise from the nature of the supported species, which results in changes in Mo=O accessibility, in activity of Mo–O-support bonds, if formed, and in the reducibility of increasing domain sizes over the specific support. The calculation of MoO_x surface densities, assuming all Mo is located at the surface, while applicable to impregnated Si : Ti supports, may be inaccurate for the "one-pot" preparation method employed for these catalysts. As discussed previously, there may be a significant amount of molybdena species located inside larger titania aggregates or deeper inside the silica network.

Faraldos *et al.* (52) linked the activity of MoO_3/SiO_2 catalysts for partial oxidation of methane to the MoO_x dispersion, noting a maximum in the rate of reducibility of the catalysts at an intermediate wt% loading before crystalline MoO_3 forms. When supported on Si : Ti 1 : 1, there is XPS evidence of Mo–O–Si linkages present at the lowest Mo wt% loading levels studied, 2 wt%. This, considered with the Raman results, suggests that at low Mo wt% loading levels, there could be isolated, monomeric MoO_x species forming on SiO_x, although molybdenum exists primarily as poly-oxo species on TiO_x, exhibiting a structure similar to what is observed on TiO_2 alone. When the loading level is increased, the amount of supported MoO_x on silica increases, leading to a more "equal" distribution between the two support phases. Reiche *et al.* (53) have observed a similar trend with vanadia grafted onto a TiO_2/SiO_2 support, in which increased loading provided a more equalized covering of Si and Ti constituents of the mixed oxide. As the Mo loading increases further, the MoO_x domains grow in size until, eventually, crystalline MoO_3 begins to form in appreciable amounts, as indicated by the XRD patterns. While these data do not explicitly differentiate between the ODH activities of Mo–O–Mo and Mo=O bonds (or reduced M^+–O centers for that matter), they do show that there is an optimum coverage of MoO_x in which several supported MoO_x species could exist together. The best catalyst may be formed at the intermediate wt% loading of Mo, where MoO_x species may be more equally distributed between the domains, sharing mixed ligands with both silica and titania; this loading consequently provides the highest ethylene yield over 10% Mo/Si : Ti 1 : 1. Furthermore, the state of the surface during ODH operating conditions is certainly a dynamic one, and several "active sites" may be responsible for favorable selectivities to ethylene during the reaction. During redox processes at the catalyst surface, linkages with the support may be rearranged and Mo species reorganized.

The current work does not examine the Mo/Si : Ti system after reaction. However, data on fresh catalysts suggest that the initial distribution of MoO_x species over the Si : Ti 1 : 1 support influences the changes that may occur during the reaction.

3.3. Ethane Temperature-Programmed Desorption

Analysis of the desorbed species after ethane adsorption on the Mo/Si : Ti 1 : 1 catalysts showed ethane, ethylene, water, methane, carbon dioxide, carbon monoxide, and trace acetaldehyde desorbing from the surface. The temperatures of desorption for various species are summarized in Table 4 where an attempt has been made to group peaks that correspond to the same temperature region. Although ethylene creates the same fragmented species as ethane in the mass spectrometer, by following specific fragments created by each, we determined that the first desorption peaks (<150°C) are associated with ethane desorption and that the remainder of the profile belongs to ethylene alone. Ethylene desorption profiles over 2 and 5% Mo/Si : Ti 1 : 1 were quite low in intensity and are multiplied by 4 in Fig. 12 for comparison to the other catalysts. In ethane TPD of the Si : Ti 1 : 1 support, there was no appreciable desorption observed, indicating that the desorbed species shown in Fig. 12 are associated with Mo sites on the catalysts. Two lower temperature desorption features of ethylene take place over 2% Mo/Si : Ti 1 : 1 at 235 and 343°C. Also, two higher temperature desorption features occur with lower intensity at 587 and 660°C. At higher wt% loadings of molybdenum, only two ethylene desorption features are present at low and high temperatures. This indicates that an additional site, present for ethylene on 2% Mo/Si : Ti 1 : 1, is missing in the other catalysts. This could possibly be

TABLE 4

Desorbed Species during Ethane TPD over Mo/Si : Ti 1 : 1 Catalysts

Catalyst	Species	Desorption temperature (°C)					
2 wt% Mo	Ethylene	235	343	587	660		
	Methane						
	Carbon dioxide			504–655			
	Carbon monoxide	284		514w[a]			
5 wt% Mo	Ethylene	204		513			
	Methane						
	Carbon dioxide		422w	518			
	Carbon monoxide	292		526w			
10 wt% Mo	Ethylene	185				519	
	Methane	186					
	Carbon dioxide			328	409	522	
	Carbon monoxide		257	321	404	520w	
15 wt% Mo	Ethylene	184				480	
	Methane	186	303				
	Carbon dioxide			314	372	487	
	Carbon monoxide		305		373	491w	
20 wt% Mo	Ethylene	176					473
	Methane	178	273sh[b]	304			
	Carbon dioxide				320	377	483
	Carbon monoxide			296		377	485

[a] w, weak.
[b] sh, shoulder.

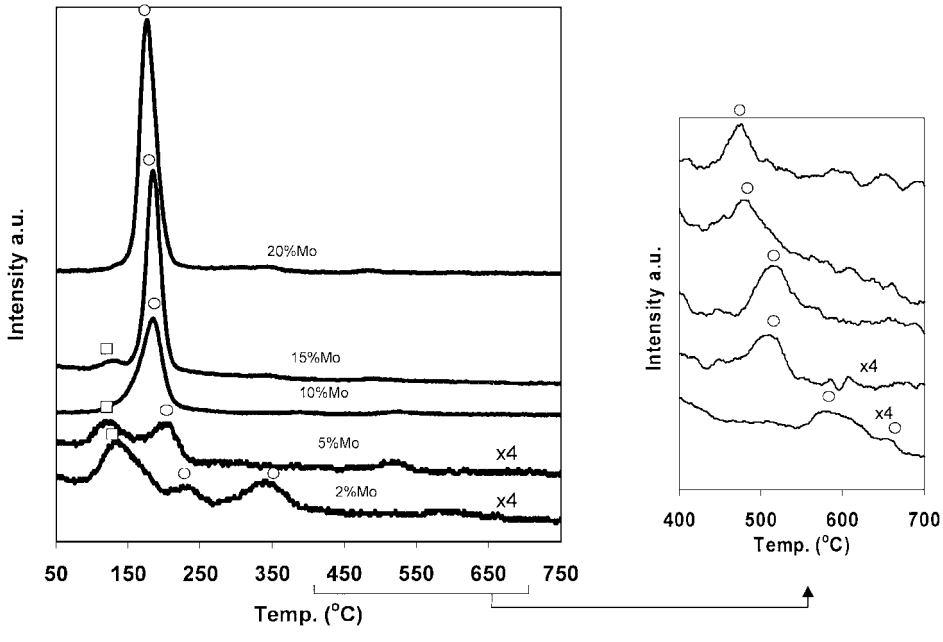

FIG. 12. Ethylene desorption profiles from ethane TPD over 10% Mo/Si : Ti 1 : 1 catalysts with different Mo wt% loadings. □, Ethane desorption; ○, ethylene desorption.

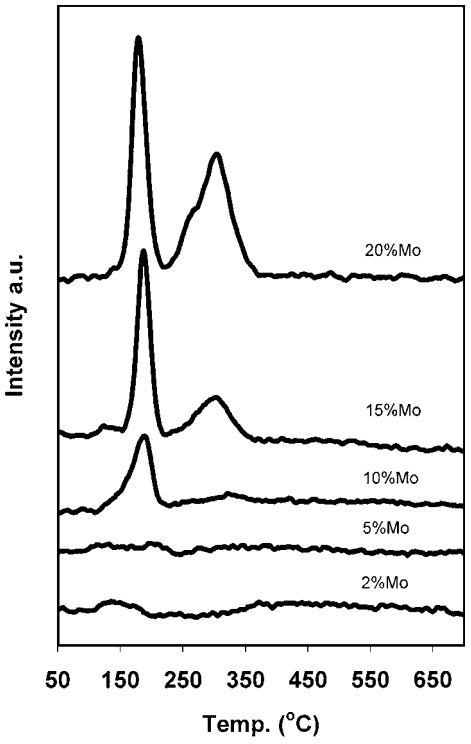

FIG. 13. Methane desorption profiles from ethane TPD over 10% Mo/Si : Ti 1 : 1 catalysts with different Mo wt% loadings.

related to the higher interaction of MoO_x in this catalyst with silica, as observed in Raman and XPS experiments. The amount of ethylene desorption is seen to be directly related to Mo content as the lower temperature desorption maxima increase in intensity with Mo wt% loading. Also, the overall desorption of ethylene is seen to shift to lower temperatures with increased Mo wt% loading (from 235 to 176°C in the low-temperature region and 587 to 473°C in the high-temperature region).

As indicated in Fig. 13, methane desorption profiles from the Mo/Si : Ti catalysts also appear to correlate with Mo wt% loading as the overall intensity is increased. No methane desorption was detected over 2 and 5 wt% Mo catalysts. As can be seen from Table 4, each low-temperature desorption feature of methane coincides with a desorption peak of ethylene over 10, 15, and 20 wt% Mo catalysts and experiences a corresponding shift to lower temperature. As the loading is increased from 10 wt%, a second, higher temperature methane desorption appears at 15 wt% (303°C) and becomes two convoluted desorption features at 20 wt% loading (273 and 304°C). This higher temperature desorption feature does not shift in temperature and must be related to the formation of crystalline MoO_3.

The desorption profiles of carbon dioxide and carbon monoxide are shown in Figs. 14a and 14b, respectively. For 2 and 5 wt% Mo catalysts, the formation of both carbon dioxide and carbon monoxide is weak and accompanies the high-temperature desorption of ethylene over these catalysts (see Table 3). Whereas methane accompanies the low-temperature desorption of ethylene over 10 and higher Mo wt% loadings, carbon monoxide is observed forming only after the low-temperature ethylene desorption for 2 and 5 wt% loadings. At 10 wt% loading of molybdenum, several sites for CO_x formation are observed that do not

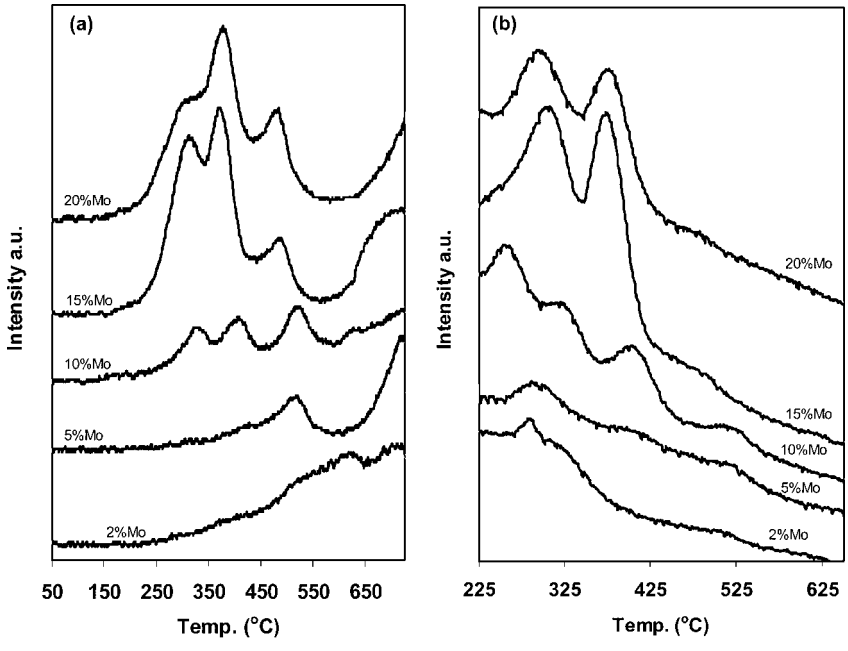

FIG. 14. (a) Carbon dioxide and (b) carbon monoxide desorption profiles from ethane TPD over 10% Mo/Si : Ti 1 : 1 catalysts with different Mo wt% loadings.

coincide with the desorptions of other species, indicating that several types of adsorbed surface complexes exist. Different oxygen species at differing activities become present on the catalyst surface at this loading. At the 15 and 20 wt% levels, CO_x desorption becomes much more intense and is accompanied by methane formation.

While TPD results cannot be directly related to behavior under reaction conditions, they elicit several important characteristics that may be relevant for catalytic behavior. The results indicate that there is a change in the catalyst surface, occurring between 5 and 10 wt% loading of molybdenum, which is responsible for the formation of several active oxygen-containing sites. However, the sites are not as active as those corresponding to crystalline MoO_3 which are present on 15 and 20 wt% samples. This could be related to an even distribution of MoO_x over silica and titania portions of the Si : Ti support present over 10% Mo/Si : Ti 1 : 1. The fact that ethylene desorption shifts to lower temperatures with increasing loading indicates that ethylene resides longer on the lowest loading catalyst. However, the formation of carbon oxides and methane is due not only to the conversion of formed ethylene but also to the transformation of the surface ethoxide intermediates into acetaldehyde, which readily converts to CO and CO_2 (54). Thus, as mentioned previously, under reaction conditions there may be several sites responsible for both the formation and the further conversion of ethylene.

4. CONCLUSIONS

The "one-pot" preparation method in which components are distributed together during gelation provided dispersed MoO_x species over the Si : Ti 1 : 1 support. However, it is quite likely that a significant amount of molybdena species may be located either inside larger titania aggregates or deeper inside the silica network. Raman spectroscopy, under ambient and dehydrated conditions, provides insight into the nature of supported MoO_x species over the Si : Ti 1 : 1 support. When considered together with the XPS data, it suggests that, at the lowest wt% loading studied, 2 wt% Mo, MoO_x may be supported preferentially on titania. However, at this same wt% loading, the presence of Mo–O–Si bonds is also detected. The interaction with the silica component of the support increases with wt% loading of molybdenum until the formation of crystalline MoO_3 occurs above 15 wt%. Combined with the fact that MoO_x species may share several types of support ligands with differing electronegativity, one cannot adequately describe MoO_x species as being supported exclusively on SiO_2 or TiO_2 domains, but rather, as indicated by the Raman results, on a mix of both species. Using this preparation method, Mo loading not only affects the structure of the surface MoO_x species but also influences the nature of TiO_x/MoO_x concentrations over the silica. As molybdenum loading is increased, there is a greater degree of crystalline titania segregation. No rutile phase was observed to form on any catalyst studied. At the same time, there appears to be an increased interaction of the silica with MoO_x.

The ethylene yield obtained in ethane ODH experiments increases with Mo loading over Si : Ti 1 : 1 to a maximum at 10% Mo/Si : Ti 1 : 1. The trend in ethane conversion and ethylene formation is accompanied by an increase in methane selectivity. The best catalyst is formed at the intermediate wt% loading of Mo, where MoO_x species may be more equally distributed between silica and titania domains or contain an optimum mix of silica and titania ligands, which consequently provides the highest ethylene yield over 10% Mo/Si : Ti 1 : 1. The ethane TPD results agree, suggesting that different oxygen species at differing activities may become available on the catalyst surface at these intermediate loadings.

ACKNOWLEDGMENTS

Financial support provided by the National Science Foundation (Grant CTS-9412544) is gratefully acknowledged. The authors also thank Mr. Chang Liu for his assistance in performing the TPD experiments.

REFERENCES

1. Baerns, M., and Buyevskaya, O., *Catal. Today* **45**, 13 (1998).
2. Cavani, F., and Trifiro, F., *Catal. Today* **24**, 307 (1995).
3. Dai, H. X., Ng, C. F., and Au, C. T., *Appl. Catal.* **202**, 1 (2000).
4. Hodnet, B. K., "Heterogeneous Catalytic Oxidation." Wiley, New York, 2000.
5. Kung, H. H., *Adv. Catal.* **40**, 1 (1994).
6. Collart, O., Van Der Voort, P., Vansant, E. F., Gustin, E., Bouwen, A., Schoemaker, Rao, R. R., Weckhuysen, B. M., and Schoonheydt, R. A., *Phys. Chem. Chem. Phys.* **A001**, 4099 (1999).
7. Gao, X., and Wachs, I. E., *Catal. Today* **51**, 233 (1999).
8. Stakheev, A. Y., Shipiro, E. S., and Apijok, J., *J. Phys. Chem.* **97**, 5668 (1993).
9. Lassaletta, G., Fernandez, A., Espinos, J. P., and Gonzalez-Elipe, A. R., *J. Phys. Chem.* **99**, 1484 (1995).
10. Walters, J. K., Rigden, J. S., Dirken, P. J., Smith, M. E., Howells, W. S., and Newport, R. J., *Chem. Phys. Lett.* **264**, 539 (1997).
11. Kumar, S. R., Suresh, C., Vasudevan, A. K., Suja, N. R., Mukundan, P., and Warrier, K. G. K., *Mat. Letters* **38**, 161 (1999).
12. Klein, S., Thorimbert, S., and Maier, W. F., *J. Catal.* **163**, 476 (1996).
13. Baiker, A., Dollenmeier, P., and Glinski, M., *Appl. Catal.* **35**, 365 (1987).
14. Vogt, E. T. C., Boot, A., van Dillen, A. J., Guess, J. W., Janssen, F. J. J. G., and van den Kerkhof, F. M. G., *J. Catal*. **114**, 313 (1988).
15. Klimova, T., Rodriguez, E., Martinez, M., and Ramirez, J., *Microporous Mesoporous Mater.* **44–45**, 357 (2001).
16. Gao, X., Bare, S. R., Fierro, J. L. G., and Wachs, I. E., *J. Phys. Chem.* **103**, 618 (1999).
17. Banares, M., Gao, X., Fierro, J. L. G., and Wachs, I. E., *Stud. Surf. Sci. Catal.* **110**, 295 (1997).
18. Gao, X., and Wachs, I. E., *J. Catal.* **192**, 18 (2000).
19. Reddy, B. M., Ganesh, I., and Chowdhury, B., *Catal. Today* **49**, 115 (1999).
20. Maity, S. K., Rana, M. S., Bej, S. K., Ancheyta-Juarez, J., Murali, D. G., and Prasada, R. T. S. R., *Catal. Lett.* **72**, 115 (2001).

21. Lakshmi, J. L., Ihasz, N. J., and Miller, J. M., *J. Mol. Catal.* **165**, 199 (2001).
22. Al-Adwani, H. A., Thammachote, N., Gardner, T. J., and Anthony, R. G., *J. Catal.* **177**, 273 (1998).
23. Miller, J. M., and Lakshmi, L. J., *J. Catal.* **184**, 68 (1999).
24. Borque, M. P., Lopez-Agudo, A., Olguin, E., Vrinat, M., Cedeno, L., and Ramirez, J., *Appl. Catal.* **180**, 53 (1999).
25. Watson, R. B., and Ozkan, U. S., *J. Catal.* **191**, 12 (2000).
26. Ozkan, U. S., Cai, Y., Kumthekar, M. W., and Zhang, L., *J. Catal.* **142**, 182 (1993).
27. Burch, R., and Crabb, E. M., *Appl. Catal.* **49**, 97 (1993).
28. Izutsu, H., Nair, P. K., Maeda, K., Kiyozumi, Y., and Mizukami, F., *Mater. Res. Bull.* **32**, 1303 (1997).
29. Watson, R. B., and Ozkan, U. S., *J. Phys. Chem.*, accepted for publication.
30. Gao, X., Bare, S. R., Fierro, J. L. G., Banarez, M. J., and Wachs, I. E., *J. Phys. Chem.* **102**, 5653 (1998).
31. Gao, X., Bare, S. R., Fierro, J. L. G., Weckhuysen, B. M., and Wachs, I. E., *J. Phys. Chem.* **102**, 10,842 (1998).
32. Armaroli, T., Milella, F., Notari, B., Willey, R. J., and Busca, G., *Topics Catal.* **15**, 63 (2001).
33. Jehng, J. M., Hu, H., Gao, X., and Wachs, I. E., *Catal. Today* **2**, 3358 (1996).
34. Quaranta, N. E., Soria, J., Corberan, V. C., and Fierro, J. L. G., *J. Catal.* **171**, 1 (1997).
35. Liu, Z., Tabora, J., and Davis, R. J., *J. Catal.* **149**, 117 (1994).
36. Weckhuysen, B. M., Jehng, J. M., and Wachs, I. E., *J. Phys. Chem.* **104**, 7382 (2000).
37. Wachs, I. E., *Catal. Today* **27**, 437 (1996).
38. Del Arco, M., Sanfelipe, M. F. M., Rives, V., Malet, P., and Ulibarri, M. A., *J. Mater. Sci.* **27**, 2960 (1992).
39. Banares, M. A., Hu, H., and Wachs, I. E., *J. Catal.* **150**, 407 (1994).
40. Banares, M. A., Hu, H., and Wachs, I. E., *J. Catal.* **155**, 249 (1995).
41. Kim, D. S., Wachs, I. E., and Segawa, K., *J. Catal.* **146**, 268 (1994).
42. Watson, R. B., and Ozkan, U. S., *Stud. Surf. Sci. Catal.* **136**, 221 (2001).
43. Fernandez, A., Leyrer, J., Gonzalez-Elipe, A. R., Munuera, G., and Knozinger, H., *J. Catal.* **112**, 489 (1988).
44. Notari, B., *Adv. Catal.* **41**, 253 (1994).
45. Stakheev, A. Y., Shpiro, E. S., and Apijok, J., *J. Phys. Chem.* **97**, 5668 (1993).
46. Reddy, B. M., Chowdhury, B., and Smirniotis, P. G., *Appl. Catal.* **211**, 19 (2001).
47. Banares, M., *Catal. Today* **51**, 319 (1999).
48. Matralis, H., Theret, S., Bastians, P., Ruwet, M., and Grange, P., *Appl. Catal. B* **5**, 271 (1995).
49. Martin, G. A., and Mirodatos, C., *Fuel Process. Technol.* **42**, 179 (1995).
50. Chen, K., Xie, S., Iglesia, E., and Bell, A. T., *J. Catal.* **189**, 421 (2000).
51. Chen, K., Xie, S., Iglesia, E., and Bell, A. T., *J. Catal.* **198**, 232 (2001).
52. Faraldos, M., Banares, M. A., Anderson, J. A., Hu, H., Wachs, I. E., and Fierro, J. L. G., *J. Catal.* **160**, 214 (1996).
53. Reiche, M. A., Ortelli, E., and Baiker, A., *Appl. Catal.* **23**, 187 (1999).
54. Kaddouri, A., Anouchinsky, R., Mazzocchia, C., Madeira, L. M., and Portela, M. F., *Catal. Today* **40**, 201 (1998).